Strong Segregation Theory of Block Copolymer−Nanoparticle Composites

Victor Pryamitsyn and Venkat Ganesan*

Department of Chemical Engineering, University of Texas at Austin, Austin, Texas 78712

Received June 15, 2006; Revised Manuscript Received September 11, 2006

ABSTRACT: We present strong segregation approximation based analytical calculations and complementary computer simulation results on the ordering and structural characteristics of block copolymer−nanoparticle mixtures. We consider specifically the case of a symmetric block copolymer organized in a lamella phase, which is mixed with both selective and nonselective nanoparticles. We present results within the strong segregation approximation quantifying the density distribution of nanoparticles and the influence of the nanoparticles upon the lamella thickness and their elastic constants. The case of nonselective nanoparticles is treated in detail to account more accurately for both size effects and finite concentrations of nanoparticles. The latter results suggest the possibility of layer instabilities and morphological transitions resulting from the surfactant-like role of nonselective particles. Qualitative features of our model predictions are in agreement with our computer simulation results.

I. Introduction

Recently there has been a surge of interest in exploiting the self-assembly in mixtures of diblock copolymers and nanosized particles to produce ordered organic−inorganic hybrid materials.[1−11] In some applications, the microphase separation of the block copolymers is used as a template to control the ordering of the particles and to produce highly organized hybrid materials.[1,2,4,12] In other applications, the particles are used to modify the self-assembly of the parent block copolymer to lead to new morphologies of self-assembly.[8,11] The resulting structures have been proposed for use in applications such as separation processes, next-generation catalysts, and photonic band gap materials.[3,12]

For successful fruition of the above applications, a fundamental understanding of the manner in which different parameters in such systems, such as the size, shape, the volume fraction of particles, the copolymer composition, and the interaction energies between the different components, control the thermodynamics and self-assembly of such nanoparticle−block copolymer mixtures. Seminal steps in this direction were taken by Balazs and co-workers, who extended the self-consistent-field theory of multicomponent polymers to include the presence of hard particles of different shapes.[13−16] Broadly, their results suggest that the templating of the particles by the block copolymer is dependent on the size of the particles and their interactions with the different units of the copolymer. If the particles were compatibilized to just one of the components (henceforth referred to as "selective" particles), then they were predicted to localize at the center of their preferred phase while particles compatible to both components (henceforth referred to as "nonselective" particles) work similar to a surfactant and localize at the AB interface of a AB diblock copolymer. An intricate interplay between selectivity and the size of the particles was also predicted. Recent computer simulations of such systems[17,19] have displayed phase behavior qualitatively consistent with these predictions. More recently, Fredrickson and co-workers have developed a hybrid particle field simulation approach,[18] which in principle can be used to study similar issues in systems involving more complex particle−polymer interactions.

The work presented in this article was motivated by two features. The first is to present an analytical treatment of ordering and thermodynamics in block copolymer−nanoparticle mixtures. Indeed, while the above studies have provided many insights into these issues, due to the cumbersome numerical formalisms, an identification of the critical parameters, scaling laws, and/or functional dependencies for different features is still lacking. In this work, we take a step toward these objectives by developing a strong-segregation approximation based theory for some of the features of block copolymer−nanoparticle composites. The second feature which motivated this study is the recent experimental observations of the bicontinuous microemulsion phases in ternary polymer blend systems,[20] which was rationalized by invoking an analogy to ternary, surfactant-oil-water mixtures. Similar observations were also noted in our simulations (presented in section 5) and in related experimental results[21] (preprint received after submission of the present article) for nonselective nanoparticle−block copolymer mixtures. These results led us to explore the analogies between block copolymer + nonselective nanoparticle systems on one hand and the surfactant based ternary systems on the other hand. Specifically, we ask, "what is the impact of nonselective nanoparticles on the block copolymer layer characteristics such as its elastic constants, and are bicontinuous phases similar to those observed in surfactants[22,23] possible by the addition of nanoparticles?" We note that strong segregation theories for block copolymer−nanoparticle composites have also been developed by Balazs and co-workers[24,25] for both the cases of selective and nonselective particles. Our work in this article is concerned mainly with neutral/slightly selective particles and in contrast to the prior research incorporates a more realistic description of the polymeric elastic free energies to develop predictions regarding block copolymer lamella phases. Moreover, we consider the possibility of lamellar phase instabilities—issues, to our knowledge, which have not been examined in prior research.

In this article, we present an analytical treatment of block copolymer−nanoparticle systems invoking the developments in the context of polymer brushes. We focus on the specific case

* Corresponding author. E-mail: venkat@che.utexas.edu.

10.1021/ma0613382 CCC: $33.50
Published on Web 10/28/2006

of symmetric block copolymers which are ordered in a lamellar structure in the absence of nanoparticles. Most recently, O'Shaughnessy and co-workers[26,27] have followed up on the earlier works of Pincus and Williams[28] to present a comprehensive treatment of some features of nanoparticle organization in polymer brushes of fixed grafting density. The first part of our work (section III) applies to both nonselective and selective nanoparticles and extends Pincus and O'Shaughnessy's works to the case of nanoparticles in block copolymer lamellae. We provide predictions for the density profiles of the nanoparticles and the impact of nanoparticles on the characteristics of the block copolymer layers. A subtle, albeit important, difference between block copolymer lamella and polymer brushes relates to the constraint of fixed grafting density invoked in brushes, but not present in block copolymers. The considerations presented in the first part are applicable only to the case of dilute concentrations of nanoparticle whose sizes are much smaller than the lamellar thickness. For such cases, we demonstrate excellent agreement with recent experimental observations. The second part of the article (section IV) focuses specifically on nonselective particles but accounts for both arbitrary concentrations and sizes of nanoparticles. We provide predictions for the changes in the lamella thickness and the elastic constants which result from the addition of nanoparticles. We comment on the possibility of layer instabilities and morphological transitions which might result from such effects. In the final section (section V), we present results of computer simulations to lend support to the predictions provided in section IV.

II. Preliminaries

In this work, we consider an AB diblock copolymer and denote the degree of polymerization of the copolymer as N and the statistical segment length as b. The unperturbed radius of gyration R_g of the copolymer is $R_g^2 = Nb^2/6$ and will be used to nondimensionalize all the length scales. All our results below will be concerned with the case of a symmetric copolymer, where the sizes of the A and B blocks are assumed to be identical. The segmental/monomeric density is denoted as ρ_0, and the nondimensional occupied volume of the polymer is denoted as $\upsilon = N/R_g^3\rho_0 = 6^{3/2}b^3\rho_0^{-1}N^{-1/2}$. Note that υ is identical to the fluctuation parameter which appears in polymer field theories, with the limit $\upsilon \rightarrow 0$ associated with the applicability of mean-field approximations.[29]

We consider the above copolymer mixed with a volume fraction Φ of nanoparticles. The nanoparticle size (in R_g units) will be denoted as R, and we will primarily be concerned with the limit $R \lesssim 1$. The interactions between the particle and the A, B components of the polymer will be quantified respectively by two interfacial tension parameters denoted η_{AC} and η_{BC}. The parameter $\delta\eta = (\eta_{AC} - \eta_{BC})$ represents the "selectivity" of the particle to the polymer component (for $\delta\eta < 0$, the particles are preferential to the A phase).

In the following, we review without proof some earlier predictions regarding the structure and properties of block copolymer interfaces and polymer brushes. We focus on the scaling predictions for the limit of strong segregations, an approximation strictly applicable only when the length scale of the interfaces becomes much smaller than the length scale of the microphase structures.[30] Explicitly, the interfacial tension at the AB polymer interface, η_{AB}, and the thickness of the AB interfaces, δ_{AB}, were calculated by Helfand and Tagami as (in nondimensionalized units)[31]

$$\eta_{AB} = \frac{\sqrt{\chi N}}{\upsilon}$$

$$\delta_{AB} = \frac{2}{\sqrt{\chi N}} \tag{1}$$

where χ denotes the Flory−Huggins interaction parameter between the A and B segments. It is also well established that, in the absence of particles, for $\chi N > (\chi N)^{(ODT)}$ melts of symmetric diblock copolymer form a lamellar structure.[32] Within strong-segregation theory, the period of the lamella structure λ is related to the height of the polymer brush formed by the AB units of the copolymer and is given as $\lambda = 2h_0$, where[30]

$$h_0 = \sqrt[3]{2\upsilon\eta_{AB}} = \sqrt[3]{2}(\chi N)^{1/6} \tag{2}$$

Weak segregation approximations and polymer self-consistent-field theories[32,33] have been used to compute the value $(\chi N)^{(ODT)} = 10.5$ and the period of the lamella at ODT as $\lambda = 3.2$ (in contrast to the value of $\lambda = 3.7$ predicted by the strong segregation approximation eq 2).

Analogies have been drawn between the organization of the A and B components in the lamella phase and the conformations of polymer brushes grafted on flat surfaces. Theoretical descriptions of polymer brushes have reached a mature state of development with many experimentally verified predictions for the cases of melt and solution brushes of polymers of a different architectures.[34−36] For the simplest case of a melt brush of a homopolymer, early theoretical descriptions were proposed by Alexander and De Gennes assuming that the free ends of all chains lie at the same height (i.e., neglects the "free-end distribution").[37,38] In such an approximation, the dimensional height of the brush h is fixed by the constraint of incompressibility, with $h = \sigma N b^3$, where σ represents the surface grafting density. Refined descriptions of polymer brushes which accounted for the "free-end distribution" were proposed independently by Semenov,[30] Milner,[39] and Zhulina[40] and their coworkers. In these models, a melt brush is predicted to have a free end distribution of the form

$$g(z) = \frac{\sigma}{h}\frac{z}{\sqrt{h^2 - z^2}} \tag{3}$$

where $g(z)$ represents the number of free ends at a distance z from the grafting surface. Moreover, the constraint of constant density is maintained within the brush through a pseudo-pressure field $P(z)$ (in k_BT units) acting on the segments of the polymer brush, where

$$P(z) = \frac{3\pi^2 h^2}{8N^2 b^5}\left(1 - \frac{z^2}{h^2}\right) \tag{4}$$

In contrast, for the Alexander−De Gennes approximation, the pressure field $P(z)$ is constant throughout the brush.

III. Dilute Concentrations of Small Selective and Nonselective Nanoparticles

In this section we consider the situation of dilute concentrations of small (quantified below) nanoparticles and relate their density distribution within the lamella to the parameters describing the polymer−nanoparticle system. For this, we first estimate the insertion energy of a single nanoparticle into the block copolymer lamella. On one hand, particles can position at the polymer−polymer interface and decrease the number of AB contacts and the contribution from AB interfacial tension.

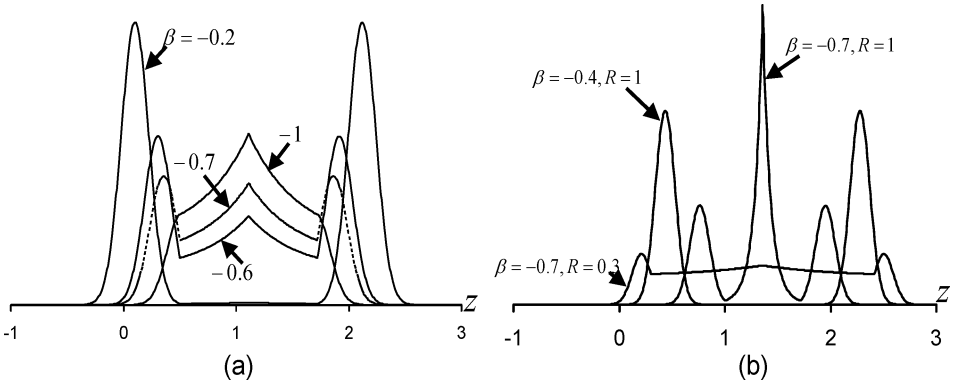

Figure 1. Typical particle density distributions $\rho_C(z)$ ($z = 0$ corresponds to the AB interface). (a) Density profiles for $R = 0.5$, $\chi N = 30$, and $\upsilon = 0.5$ for different selectivity parameters β. (b) Density profiles for different β and R combinations at $\chi N = 100$ and $\upsilon = 0.5$.

Alternatively, the particles can position itself in its preferred phase, which leads to an enthalpic gain in free energy. Finally, the presence of nanoparticles in the lamellar "brush" leads to an increase in the elastic free energy of the brush which depends on the position of the nanoparticle. By estimating the interplay between these effects, we determine the density distributions of the nanoparticles.

To estimate the increase in elastic free energy, we draw upon the results of earlier works of Williams and Pincus[28] and the more recent work of O'Shaughnessy and Kim.[26,27] These researchers considered the case of small nanoparticles placed in polymer brushes and have shown that the polymeric elastic energy cost ΔE_{br} arising from the placement of a single nanoparticle at a location z inside the brush can be determined approximately as

$$\Delta E_{br}(z) \simeq P(z)\frac{4\pi R^3}{3} \tag{5}$$

where $P(z)$ denotes the pressure field discussed earlier (eq 4). This approximation is expected to be valid when the perturbation caused by the nanoparticle is weak on the scale of the polymer brush, which corresponds to particles much smaller than the polymer brush. (O'Shaughnessy[27] has argued that the relevant length scale controlling the nanoparticle perturbation is the size of the elastic blob. However, for the diblock copolymer lamella, the distinction between the elastic blob and brush height is not significant until extremely high χN.) For the case where the nanoparticle is located in a diblock copolymer lamella, we adopt the convention that the AB interface is located at $z = 0$ and that the A polymers occupy $z > 0$. The height of the brush is then replaced by one-fourth the thickness of the lamella (eq 2), and the above can be expressed as

$$F_{br}(z) = \frac{h_0^{\,2}\pi^3 R^3\left(1 - \dfrac{4z^2}{h_0^{\,2}}\right)}{48\upsilon} \tag{6}$$

The interfacial cost arising from placing the nanoparticle at a location z is

$$F_{enth}(z) = \begin{cases} \pi(z^2\eta_{AB} + 2Rz\delta\eta), & |z| \le R \\ \pi R^2\left(\dfrac{2z\delta\eta}{|z|} + \eta_{AB}\right) & |z| > R \end{cases} \tag{7}$$

In eq 7, the two distinct cases arise from the reduction in the AB interface when the particle is such that $|z| < R$ and the lack of such an effect for $|z| > R$.

A. Density Distributions. Using eqs 6 and 7, we can approximate the density distribution of nanoparticles $\rho_C(z)$ in the diblock lamella as

$$\rho_C(z) \propto \exp[-F_{enth}(z) - F_{br}(z)] \tag{8}$$

Equation 8 is seen to be dependent on four distinct parameters: χN, υ, R (where υ is a measure of the number of segments in the polymer N), and $\beta = \delta\eta/\eta_{AB}$. We note that β^{-1} quantifies the degree of amphiphilicity or the surfactant-like nature of the particle. The qualitative features of the above density distribution are displayed in Figure 1. It is seen that for a fixed χN, υ, and R small values of β lead to a localization of the particles at the AB interface of the copolymer. In contrast, increasing the selectivity of the particles leads to a delocalization of the particles into its preferred phase. Interestingly, we observe that for intermediate values of selectivity the overall density distribution displays three peaks corresponding to a localization at the middle of the brush in its preferred phase. The latter is a manifestation of the lower elastic energetic cost (cf. eq 6) associated with being present at the top extremities of a polymer brush compared to its interiors.

Prior to quantifying the localization of the particles, we discuss the relationship between the above predictions and related experimental results. The most striking confirmation of our theoretical predictions is provided by the recent experiments of Kim et al.[9] These experiments considered the organization of gold nanoparticles whose selectivity to one of the phases was controlled grafting its surface with shorter chains of one of the polymers. Results (Figure 4 of ref 9) specifically indicated the occurrence of a single peak in the density distribution at high values of selectivity (similar to $\beta = -1$ in Figure 1), and with decreasing selectivity, the density distribution evolves toward a profile with three peaks and finally toward a distribution with just two peaks localized at the AB interface.

Other experiments have considered the role of the size of the particles in influencing the ordering of *selective* particles within its preferred phase.[1,7] Overall, small selective particles have been found to be more localized at the AB interface, whereas the larger particles tend to exhibit more preferential segregation. These results are also seen to be consistent with the physical ideas underlying our analysis. Indeed, for selective particles, there are three competing energetic effects: (i) the decrease in AB interfacial tension arising from the localization at AB interface; (ii) the enthalpic gain in localizing into the A (or B) domains; (iii) the reduction in polymer elastic penalty by localizing in the middle of the A (or B) domains. From eqs 6 and 7, it is evident that the first two contributions scale as R^2 (surface area), whereas the third contribution scales as R^3 (the

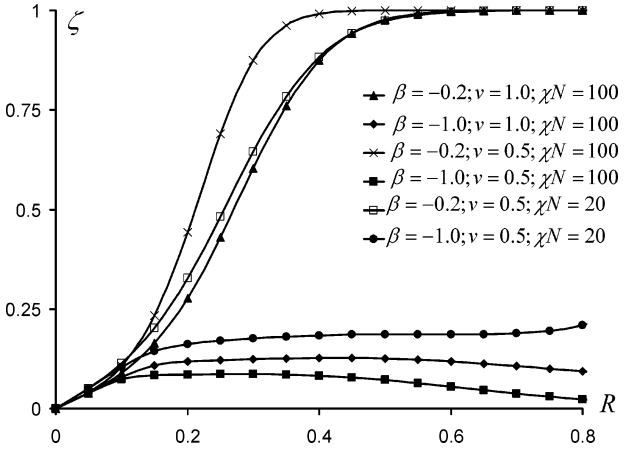

Figure 2. Fraction of particles which are localized at the interface (eq 9) for different parametric conditions.

volume of the particle). Consequently, for small particles and/or for stronger segregation between A and B phases (i.e., larger AB interfacial tension), the particles can be expected to be more localized at the AB interface. In contrast, for larger particles and/or weaker segregations, the tendency to segregate into the preferred domain dominates. More interestingly, these considerations emphasize the subtle interplay of size with other effects such as the degree of segregation in influencing the overall density distributions. These effects are clearly illustrated in Figure 1b, which illustrates the role of size in the density distributions for a specific parametric choice of selective and nonselective particles.

An explicit measure of the surfactant-like nature of the particle is provided by the probability of localization at the interface ζ, defined as

$$\zeta = \frac{\int_{-R}^{R} \mathrm{d}z\, \rho_C(z)}{\int_{-h_0/2}^{h_0/2} \mathrm{d}z\, \rho_C(z)} \tag{9}$$

and is displayed in Figure 2. It can be observed that a fixed selectivity β, decreasing υ (equivalently, increasing N), and/or increasing χN increases the AB interfacial tension and thereby leads to a more pronounced interfacial localization of the particles. Moreover, it is also seen that for weakly selective particles an increase in the particle size leads to an increase in the localization of the particles, but in contrast, strongly selective particles display a maximum in interfacial localization at an intermediate size, while exhibiting a reduced localization at larger sizes. The latter trends are consistent with our earlier discussion.

B. Lamella Thickness. In contrast to the case of polymer brushes, the grafting density is not *a priorily* fixed for block copolymers. While the results in the previous section assumed that h_0 corresponded to its equilibrium, unperturbed value, the introduction of the particles can change the characteristics of the block copolymer layers such as the lamella thickness, elastic constants, etc. Here we consider the impact of nanoparticles upon the lamella thickness in block copolymers (the elastic constants are addressed in the next section). The latter has been experimentally characterized using neutron reflectivity measurements[7] and has also been used as an indirect measure of the localization characteristics of the particles. The equilibrium lamella thickness (denoted $2h$) in the presence of nanoparticles can be obtained by combining the free energy arising from the density distribution of the nanoparticles with the free energy of the diblock copolymer brush. For a volume fraction Φ of particles, we obtain the free energy (on a per chain basis) as

$$F = \frac{\pi^2 h^2}{48} + \eta_{AB}\frac{\upsilon(1+\Phi)}{h} + \frac{3\upsilon\Phi}{4\pi R^3}\ln \Xi \tag{10}$$

In eq 10, the first term represents the elastic free energy of a parabolic brush[30] and the second term quantifies the AB interfacial energy cost (on a per chain basis). The last term, where

$$\Xi(h) = \left[\frac{1}{h}\int_{-h}^{h}\rho_C(z)\right]^{-1} \tag{11}$$

represents the ideal gas free energy associated with the density distribution of the particles [$\rho_C(z)$ given by eq 7].

The lamella thickness can be obtained by minimizing the above free energy with respect to the h. Since the approximations used in the present section are expected to be valid only when the interparticle interactions are neglected, we just provide the leading order correction in Φ expanded to the first few terms in the size of the particle R:

$$\frac{h-h_0}{h_0} = \Phi\left[-\frac{11}{12} + \frac{2\pi R^2(-1+5\beta^2)\sqrt{\chi N}}{15\upsilon}\right] \tag{12}$$

For the limit $\beta \to 0$, we observe that

$$\frac{h-h_0}{h_0} = -\Phi\left[\frac{11}{12} + \frac{2\pi R^2\sqrt{\chi N}}{15\upsilon}\right] \tag{13}$$

indicating that there is a contraction of the lamella thickness due to the addition of particles. The latter can be physically understood as arising from the reduction in the AB interfacial costs arising from the positioning of the particles at the interface. Whence, the chains have to stretch less to accommodate the unfavorable AB contacts. In contrast, for the limit $\beta \gg 1$, it can be seen that

$$\frac{h-h_0}{h_0} = \Phi\left[\frac{2\pi R^2\beta^2\sqrt{\chi N}}{3\upsilon}\right] \tag{14}$$

indicating a swelling of the lamellae, a characteristic similar to that seen during the addition of a selective solvent. Overall, it can be seen that the degree of swelling or contraction are also in general dependent on the degree of segregation (parameters χN and υ) and the size of the particle R in addition to the dependence on the selectivity parameter β.

The above trends already point to possibly interesting effects upon the elastic constants of the block copolymer layers, the second issue of interest in this article. Indeed, for pure block copolymer lamella, the elastic constants are correlated to the thickness of the layer[41] and are hence expected to be modified by the addition of particles. While in principle it is possible to use the same approximation above to also calculate these effects, the resulting expressions prove more cumbersome. Since such issues are typically of interest for the case of surfactant-like particles, in the next section we consider an approximation which is expected to be accurate for weakly selective or nonselective particles, but one that can also include the effect of *nondilute concentrations and larger sizes* of particles to compute the change in elastic constants of the layer.

In summary, a simple energetic argument is seen to predict the qualitative features of the density distributions of the nanoparticles in the block copolymer layers. However, the

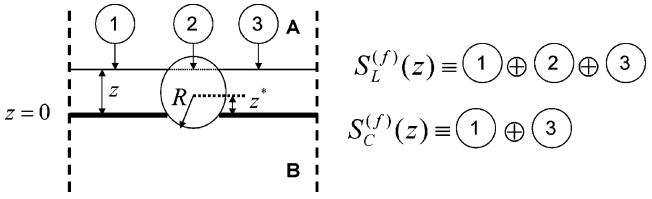

Figure 3. Schematic of the particle−polymer periodic cell. A and B denote the components of the block copolymer, and $z = 0$ corresponds to the AB interface. The geometrical notations are explained in the text.

arguments used in this section are strictly applicable only in the limit of dilute concentrations of nanoparticles for which eqs 5 and 7 are applicable. To address the impact of larger sizes and finite concentrations of nanoparticles (where the particles can "see each other" through the polymers) upon the ordering and properties of the block copolymer layers requires an extension of eq 5 to address the influence of nanoparticles on the characteristics of polymer brushes themselves. This problem is complex, requiring in general the solution of self-consistent-field equations for the polymer brush in the presence of fixed boundaries (corresponding to the fixed locations of particles).[27] However, for the specific case of weakly selective particles, in the next section we exploit the localization of the particle near the AB interface to derive an approximate expression quantifying these effects.

IV. Weakly Selective and Nonselective Particles

For the case of the weakly selective ($\beta \approx 0$) and nonselective ($\beta = 0$) particles, the density profiles displayed in Figure 1 indicate that the particles tend to be localized near the interface. An important feature of the chain conformations near the grafting surface (cf. eq 3) is the relative lack of free ends. As an approximation, the free end distribution of the chains can be ignored, and an extension of the Alexander−DeGennes approximation can be used to compute the height of the brush and the effect of the particles upon the elastic constants of the block copolymer layer. To further simplify the algebraic details, we make another additional, albeit not strictly necessary, approximation, wherein we posit that the particles are all localized at a fixed position z^* corresponding to the peak in their density distributions. In such a case, we neglect the translational entropy contribution arising from the delocalization of the particles normal to the interface. The "strong localization" approximation is expected to be accurate for the case where the particle sizes are not too small (cf. Figure 2), which is the parameter regime considered in this section. In such a case, we consider a volume fraction ϕ of the particles localized near the interfacial position, where ϕ is related to the overall volume fraction Φ of the particles through the coefficient ζ (eq 9) as $\phi = \zeta\Phi$.

To compute the free energy of the brush and the changes in elastic constants at finite concentrations of particles, we use a cell approximation where we calculate the free energy of a periodical cell containing one particle and N_c copolymer chains (see Figure 3), with

$$N_c = \frac{4\pi R^3(1-\phi)}{3v\phi} \tag{15}$$

The total volume of the cell is then $V = N_c v + {}^4/_3\pi R^3$. We then consider a spherical particle of radius R placed at a position z^* near the AB interface of flat, cylindrically and spherically bent cells. The radius of curvature of the cylindrical and spherical cells are denoted as $\mathscr{R}$, and our considerations will be restricted to $\mathscr{R} \gg R$. The area of the cell (including the particle) at any height z will be denoted as $S_L^{(x)}(z)$, where x = f, c, and s respectively for the flat, cylindrical, and spherical brush configurations. The area at the AB interface ($S_L^{(x)}(z = 0)$) is specifically denoted as $S_0^{(x)}$. The area of the cell at a height z excluding the particles is denoted as $S_C^{(x)}(z)$ (x = f, c, s) (cf. Figure 3).

On the basis of simple geometrical constructions, the following formulas can be derived:

(i) For the flat brush:

$$S_L^{(f)}(z) = S_0^{(f)}$$

$$S_C^{(f)}(z) = S_0^{(f)} - \pi(R^2 - (z - z^*)^2) \tag{16}$$

(ii) For the cylindrical brush:

$$S_L^{(c)}(z) = S_0^{(c)}\left(1 + \frac{z}{\mathscr{R}}\right)$$

$$S_C^{(c)}(z) = S_L^{(c)}(z) - \pi(R^2 - (z - z^*)^2)\left[1 + \frac{(z - z^*)}{2\mathscr{R}} + \frac{(R^2 - (z - z^*)(5z + 11z^*))}{32\mathscr{R}^2} - O[\mathscr{R}^{-3}]\right] \tag{17}$$

(iii) For the spherical brush:

$$S_L^{(s)}(z) = S_0^{(s)}\left(1 + \frac{z}{\mathscr{R}}\right)^2$$

$$S_C^{(s)}(z) = S_L^{(s)}(z) - \frac{\pi(R^2 - (z - z^*)^2)(z + \mathscr{R})}{z^* + \mathscr{R}} \tag{18}$$

A key quantity in determining the elastic free energy of the brush the Alexander−DeGennes approximation is the area available for the polymer chains ($S_C^{(x)}$).[30] To determine the latter and the elastic free energies, we require expressions for $S_0^{(x)}$ and the heights of the brushes $h_1^{(x)}$ and $h_2^{(x)}$. These are given by the solution of the following implicit equations:

$$N_C v + \frac{4}{3}\pi R^3 = \int_{-h_2^{(x)}}^{h_1^{(x)}} S_L^{(x)}(z)\, dz \tag{19}$$

$$\frac{1}{2}N_C v = \int_0^{h_1^{(x)}} S_C^{(x)}(z)\, dz \tag{20}$$

$$\frac{1}{2}N_C v = \int_{-h_2^{(x)}}^{0} S_C^{(x)}(z)\, dz \tag{21}$$

and the total height of the brush is given as $h^{(x)} = h_1^{(x)} + h_2^{(x)}$. The first of the above equations embodies the conservation of total volume, while the second and third equations represent the conservation of the volumes of A and B chains. The above equations were solved in conjunction with eq 15 using a symbolic computation package to determine $S_0^{(x)}$, $h_1^{(x)}$, and $h_2^{(x)}$ in terms of ϕ, $h^{(x)}$, and R.

The elastic free energy of the polymer layer per particle can be calculated from strong stretching approximation:[30]

$$F_e = \frac{3}{2}b^2 N_c \int_0^{N_p}\left(\frac{\partial R(n)}{\partial n}\right)^2 dn = \frac{{N_c}^2 v}{4}\int_{-h_2^{(x)}}^{h_1^{(x)}} \frac{dz}{S_C^{(x)}(z)} = \frac{4\pi^2 R^6(1-\phi)^2}{9v}\int_{-h_2^{(x)}}^{h_1^{(x)}} \frac{dz}{S_C^{(x)}(z)} \tag{22}$$

In eq 22, $R(n)$ denotes the spatial coordinate of a polymer segment n. The total free energy per cell F_t can then be obtained by combining the above free energy contribution with the enthalpic free energy identified in eq 7:

$$F_t(h^{(x)}, z^*, \phi, \mathscr{R}) = F_e + S_C^{(x)}(z=0)\eta_{AB} + 2\pi R z^* \delta\eta + F_{tran} \quad (23)$$

(We ignore the possibility $z^* > R$, since we are specifically considering surfactant-like localized particles.) The last term in eq 23 is the 2D translational entropy of the localized particles:

$$F_{tran} = -\log[S_C^{(x)}(z=z^*)] \quad (24)$$

To calculate the thickness and associated characteristics of the layers requires minimization F_t in eq 23 over both $h^{(x)}$ and z^*. The elastic constants can then be obtained from the leading order terms in an expansion in the curvature radius $\mathscr{R}$ of the minimum free energies $F_t^{(c)}$ and $F_t^{(s)}$ of the cylindrical and spherical brushes:[41,42]

$$F_t^{(c)} = F_t^{(f)} + \frac{c_0}{2\mathscr{R}} + \frac{K}{2\mathscr{R}^2} \quad (25)$$

$$F_t^{(s)} = F_t^{(f)} + \frac{c_0}{\mathscr{R}} + \frac{2K+\bar{K}}{\mathscr{R}^2} \quad (26)$$

where c_0 denotes the spontaneous curvature of the layer, K and $\bar{K}$ denote the bending modulus and saddle-splay modulus of the layer, and $F_t^{(f)}$ represents the free energy of the flat layer.

A dimensional analysis suggests that the influence of the particles is governed by two parameters: (i) $\alpha = R/h_0$, which quantifies the size of the particle relative to the initial (unperturbed) size of the lamella; (ii) $\delta = \upsilon R^{-3}(\chi N)^{-1/3}$, representing the effect of fluctuations on the scale R. In eq 23, the elastic and enthalpic terms are independent of δ, whereas the contribution of F_{tran} is controlled by the fluctuation parameter δ. In the following section, we first consider the limit where $\delta \ll 1$, for which the results are simpler, and we present analytical and numerical results for the block copolymer layer characteristics. The limit where $\upsilon R^{-3}(\chi N)^{-1/3}$ is arbitrary leads to more cumbersome analytical expressions. For such a limit, we consider only selected characteristics and present mainly numerical and some leading order analytical results.

Results for $\upsilon R^{-3}(\chi N)^{-1/3} \ll 1$. *1. Location of the Particle.* For the flat interface, it is possible to obtain an analytical expression for the preferred location of the center of the localized particle:

$$z^* = -\frac{2R\upsilon\delta\eta}{h_0^3} \quad (27)$$

which is independent of the particle concentration ϕ. Using eq 27, a self-consistent condition can be derived for the parametric regime over which the particle behaves similar to a surfactant (i.e., $z^* < R$):

$$\frac{h_0^3}{2\upsilon} > |\delta\eta| \quad (28)$$

Upon using (1), we observe that for $\beta = |\delta\eta|/\eta_{AB} > 1$ the particle loses its surfactant-like properties.

2. Brush Thickness and Lamella Period. Minimization of free energy eq 23 over h gives us the height of the brush and lamella period as a function of interfacial concentration ϕ. Up to $O[\phi^4]$, we obtain

$$\frac{h(\phi)}{h_0} = 1 + \frac{\phi}{3} - \left(\frac{3}{10\alpha} - \frac{5}{9}\right)\phi^2 - \left(\frac{9}{35\alpha^2} - \frac{1}{10\alpha} - \frac{23}{81}\right)\phi^3 - \left(\frac{3}{14\alpha^3} - \frac{27}{100\alpha^2} + \frac{7}{15\alpha} - \frac{107}{243}\right)\phi^4 + O(\phi^5) \quad (29)$$

where $\alpha = R/h_0 = R/\sqrt[3]{2}(\chi_{AB}N_p)^{1/6}$. It is seen that the coefficient of the linear term ϕ in eq 29 is positive, suggesting a swelling of the layers due to the addition of nonselective particles. While this appears contradictory to the result in the previous section, we note that we have neglected the particle translational entropy contributions in deriving eq 29. In the next section, we demonstrate that incorporating the translational entropy of the particle does lead to a contraction of the lamella for small particles even at the leading order in ϕ. Second, it is also seen that the change in brush height is independent of the selectivity parameter β. The origin of this feature can be traced to neglecting the effect of free end distributions in our model. For such an approximation, the pressure field acting on the particle is independent of its position and the selectivity parameter β.

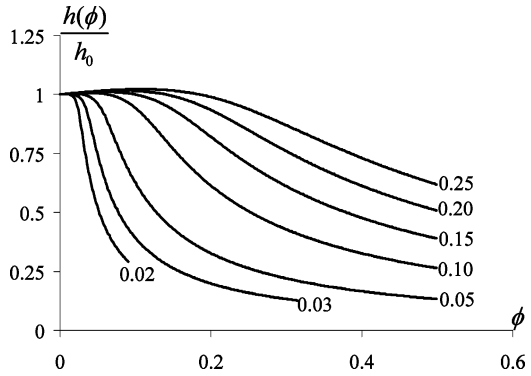

Figure 4. Height of the A brush as a function of interfacial particle concentration ϕ for different values of $\alpha = R/h_0$.

More pertinent is the overall ϕ dependence of the height, the numerical nonperturbative result for which is displayed in Figure 4. It is observed that over almost the entire range of volume fractions our model predicts a decrease in the size of the lamellar thickness upon the addition of particles. As elaborated earlier, this effect can simply be understood as arising from the particle-induced reduction in the AB interfacial costs. This effect is seen to become more pronounced with an increase in the concentration of the particles ϕ and with a decrease in the size of the particles. The latter can be understood by noting that, for a given concentration ϕ at the interface, smaller particles lead to less elastic distortion costs for the polymer (polymers have to deviate less to avoid the particles). Second, since the total surface area of the smaller particles are much larger than that of larger particles, by positioning at the interface, smaller particles provide more enthalpic gain. Together, these effects cause a more stronger reduction in the height of the brush at a specified ϕ.

With the strong contraction in the brush height predicted in Figure 4, at a critical ϕ the height of the brush is expected to become $h(\phi) < R_g$, corresponding to an overall compression of the polymer chains. It is known from other contexts that compression of polymer chains in brush systems can cause the development of lateral instabilities in the brushes.[43−45] In the present context, one can can expect that the copolymer lamella structure would lose its stability if the thickness of lamella become less them R_g. In a later section we discuss such instabilities in more detail.

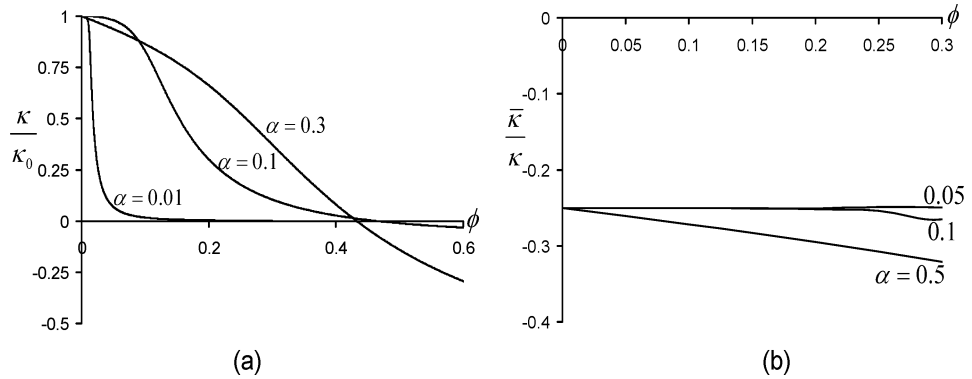

Figure 5. (a) Numerical, nonperturbative values of bending modulus of the lamella κ (normalized by its value in the absence of particles, κ_0) as a function of ϕ for different $\alpha = R/h_0$. (b) Perturbative values of saddle-splay modulus of the lamella $\bar{\kappa}$ normalized by κ) as a function of ϕ for different $\alpha = R/h_0$.

3. Elastic Constants. The particle-induced spontaneous curvature c_0 (the original diblock copolymer being symmetric has no inherent spontaneous curvature) can be determined to $O(\phi^2)$:

$$c_0 = \frac{-3\beta(\beta^2 + h_0^4(8\alpha + 3))\phi}{8h_0^7} + O(\phi^2)$$

Interestingly, for $\alpha \ll 1$

$$c_0 \approx -\frac{9\beta\phi}{8h_0^3} + O(\phi^2)$$

suggesting that the addition of even infinitesimally small particles can induce a spontaneous bending of the layer of the block copolymer brush. The above expression suggests that even in a symmetric lamella, the addition of particles has an effect equivalent to inducing a positive curvature in the direction of its preferred phase.

The bending modulus κ and the saddle-splay modulus $\bar{\kappa}$ can be obtained as (to $O(\phi^3)$)

$$\frac{6v}{h_0^5}\kappa = 1 - \left(\frac{1}{3} + \frac{63\alpha}{64} + \frac{3\alpha^2}{10} + 2\alpha^3\right)\phi + \left(\frac{14}{9} - \frac{3}{2\alpha} + \frac{393\alpha}{448} - \frac{3\alpha^2}{10} + \frac{14\alpha^3}{3}\right)\phi^2 \quad (30)$$

and

$$-\frac{24v}{h_0^5}\bar{\kappa} = 1 - \left(\frac{1}{3} + \frac{9\alpha}{8} - \frac{12\alpha^2}{5}\right)\phi + \left(\frac{14}{9} - \frac{3}{2\alpha} + \frac{57\alpha}{40} - \frac{12\alpha^2}{5}\right)\phi^2 \quad (31)$$

For $\phi = 0$, the scaling of the above expressions eqs 30 and eqs 31 is in agreement with that calculated by Milner and Witten.[41] The volume fraction dependencies of the elastic constants are displayed in Figure 5a,b, wherein the bending modulus results correspond to the nonperturbative numerical values, whereas the saddle-splay modulus values correspond to the above perturbative results and are displayed as the ratio $\bar{\kappa}/\kappa$. The latter representation is motivated by membrane stability considerations which typically require both $\bar{\kappa} < 0$ and $\bar{\kappa} + 2\kappa > 0$ for the stability of lamellar membranes. From Figure 5 it is seen that the addition of particles decreases the bending modulus and increases the saddle-splay modulus of the layers. Moreover, smaller particles are again seen to lead to more significant changes compared to the larger particles. These effects are consistent with the observations related to the changes in the height of the brush, where upon addition of particles the AB interfacial cost is relieved, resulting in less cost for bending the brushes. Interestingly, our results predict the possibility that the bending modulus κ can become zero or negative (and correspondingly $\bar{\kappa} \geq 0$). Using eq 30, it is possible to estimate a critical particle concentration ϕ_κ where the bending modulus becomes zero:

$$\phi_\kappa \approx 0.8\sqrt{\alpha} - 0.1\alpha + O(\alpha^{3/2}) \quad (32)$$

Since $\kappa < 0$ typically corresponds to unstable state for fluctuations of the interface,[46,47] its occurrence is expected to lead to a morphological transition from the lamellar state. We discuss these effects in the next section.

4. Instabilities Due to Brush Height and Bending Modulii. In the previous sections, we presented results for the influence of particles upon the height and the elastic constants of the block copolymer layer. In these contexts, two observations were noted, viz., the decrease in brush height and a trend toward unstable values of the elastic constants. In this section, we point out that each of these effects can potentially lead to an instability of the lamellar system and to a morphological transition. We analyze the relative locations of these instabilities to determine a stability "phase diagram" for the system.

We first discuss the instability arising from the brush contraction. In a laterally homogeneous lamella, typically the height of the brush h is larger than the radius of gyration of the component R_g^L (stretched chains), for which case the elastic free energy of stretching of the polymer chain $f_{el} \propto h^2/(R_g^L)^2$. The area of AB interface per chain is proportional to h^{-1} (incompressibility constraint), and the interfacial free energy per chain is $\delta f_{int} \propto \eta_{AB} h^{-1}$. Minimization of $\delta f = \delta f_{el} + \delta f_{int}$ yields the equilibrium value of the lamellar thickness h. In contrast, if $h < R_g^L$, the chain becomes compressed, and the elastic free energy is no longer proportional to h^2. Other researches in the context of polymer brushes have considered similar situations as above to suggest the development of lateral inhomogeneities to relieve the unfavorable cost of chain compression (Figure 6).[43,44] For our system, the deformation of a chain along the contour is in reality inhomogeneous. Near the AB interface, polymer chains are squeezed by the particles and are hence always stretched. However, there is an external region to the brush where, depending on the particle concentration, the polymer segments may be stretched or compressed. If those segments are also stretched, the lamella structure is expected to be stable. Whereas, if they are compressed, we then

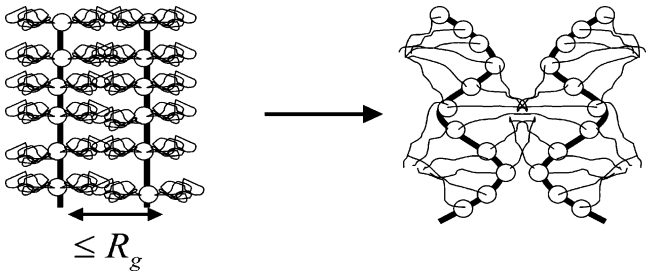

Figure 6. A cartoon of the potential instability due to compression of the brush. The left-hand panel depicts the initially unfavorable configuration of compressed brush. The right-hand panel depicts the manner in which undulations can relieve the compression of chains.

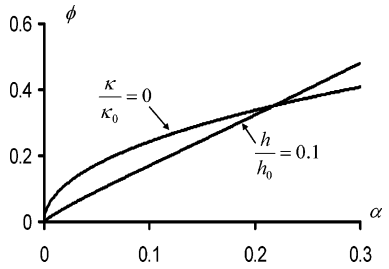

Figure 7. Critical lines in the interfacial concentration $\phi-\alpha$ plane for instabilities relating to the bending modulus and the height of the brushes. Regions above the lines correspond to unstable regimes.

expect that the lamella to become laterally undulated to relieve the chains from unfavorable compression.

While the above instability is specific for a copolymer system, in the context of surfactant solutions, instabilities (and specifically the formation of bicontinuous L_3 phases) have been associated with the bending modulus $\kappa \ll 1$ and the saddle-splay modulus $\bar{\kappa} \approx 0$.[22,23,46] In the preceding section, we noted that beyond a critical particle concentration such a situation can occur also in the context of nanoparticle−block copolymer mixtures. In such situations, we expect the block copolymers to resemble surfactant bilayers and result in bicontinuous structures similar to L_3 phases.

In Figure 7 we display a "phase diagram" for the onset of the above instabilities in coordinates of interfacial particle concentration ϕ vs relative particle size $\alpha = R/h_0$. One can see that for the model considered here, for $\alpha \lesssim 0.25$, the instability related to the lamella compression (arbitrarily chosen to occur at the volume fraction at which $h/h_0 = 0.1$) occurs at lower particle concentrations compared to the instability arising from the bending modulus. The latter can be understood by noting that for small α the critical volume fraction for the brush instability scales as α, whereas (cf. eq 32) $\phi_{(\kappa)} \propto \alpha^{1/2}$. In contrast, for larger values of the α parameter, the instability resulting from the bending modulus precedes that arising from the lamella compression.

A disadvantage of our approach is that while we can identify the trends toward the onset of morphological instabilities, we lack the means to identify the resulting phase structures. However, by analogy to surfactant solutions, it is likely that these instabilities lead to a structurally disordered state which is still microphase separated rather than a phase mixed disordered state. Moreover, while the above discussion suggests that accumulation of the particles at the interface can cause an instability, caution should be exercised in drawing quantitative conclusions based on the strong segregation theory approach used in this article. Recently, it was pointed out by Matsen[42] strong segregation theory becomes quantitatively reliable for the calculation of block copolymer characteristics only for $\chi N > 10^5$. For weaker segregation regimes, our estimate of κ could be significantly higher than the actual value, thereby shifting the instability line due to bending modulus toward lower particle concentrations.

Finally, much of our above discussion used the interfacial concentration ϕ to identify the effects of nanoparticles. In such a context, smaller particles were always seen to act as better surfactants. However, as Figure 2 indicates, smaller particles also tend to exhibit a more delocalized density distribution which is not accounted within our "strongly localized" model. A crude way to incorporate these effects is to relate ϕ to the overall particle concentration Φ through the parameter ζ as $\phi = \zeta\Phi$. (To be consistent, we recomputed ζ in the Alexander−DeGennes approximation, instead of the parabolic approximation used in section III.) To illustrate the qualitative trends resulting from this renormalization, Figure 8 displays, in the $\Phi-R$ plane and at different values of υ and χN, the region over which the lamellar region is stable to the height instabilities. Overall, it is seen that the transformation from ϕ to Φ mainly affects the results for small R, wherein in this representation smaller particles cease to be efficient surfactants. A lowering of υ causes an increase in the localization of the particles, leading to an expansion of the region of lamella instability for smaller R. Similarly, an increase of χN also causes an increase (much weaker) in η_{AB} and correspondingly an expansion of the region of lamella instability for small particles.

B. Results for Arbitrary $\upsilon R^{-3}(\chi N)^{-1/3}$. The previous sections considered for simplicity the results for the case where the 2D translational entropy of the particles were neglected. In this section, we discuss the results for arbitrary values of $\delta = \upsilon R^{-3}(\chi N)^{-1/3}$. In many cases, the resulting analytical results tend to be more cumbersome expressions, and so we mainly discuss the characteristics of the lamella thickness and the bending modulus κ and present the corrections to the leading order terms and display the corresponding numerical results. Our numerical results consider the situation where R and χN are fixed, where the influence of the parameter δ appears through the role of the fluctuation parameter υ.

With the inclusion of the fluctuation corrections, the lamella thickness of eq 29 becomes

$$\frac{h(\phi)}{h_0} = 1 + \left(\frac{1}{3} - \frac{2\delta}{3}\right)\phi + \left(\frac{5}{9} - \frac{3}{10\alpha} - \frac{4\delta}{9}\right)\phi^2 + O(\phi^3) \quad (33)$$

Figure 9 illustrates the role of fluctuations by displaying the complete numerical dependency of the brush height (for $\upsilon = 1$) as a function of the concentration of the particles ϕ. It is evident that the inclusion of the translational entropy contributions tends to lower the lamella thickness even further compared to its value in the absence of fluctuations. The latter can be rationalized by noting that additional entropic gain of the particles reduces even further the overall free energy cost of the lamella. The fluctuation corrections to the bending modulus κ (displayed in Figure 9b) can also be derived in a perturbative manner:

$$\frac{6\upsilon}{h_0^5}\kappa = 1 - \left(\frac{1}{3} + \frac{63\alpha}{64} + \frac{3\alpha^2}{10} + 2\alpha^3 + \left(\frac{10}{3} + 3\alpha^2 + 8\alpha^3\right)\delta + 8\alpha^3\delta^2\right)\phi + O(\phi^2) \quad (34)$$

Similar to the effects noted in lamellar thickness, we observe an additional lowering due to the translational entropy of the particles. However, overall it is seen that the impact of the parameter δ is mainly quantitative and does not impact the qualitative features of our earlier results. The same conclusion was

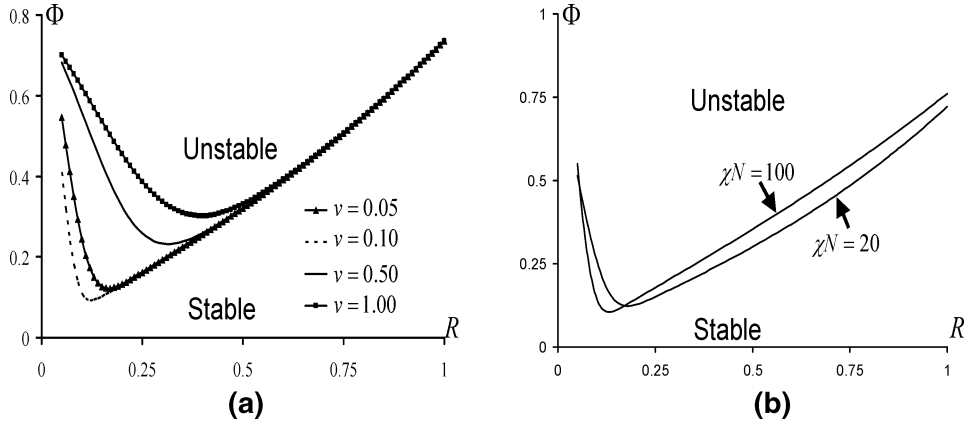

Figure 8. Critical lines for brush compression instability in the $\Phi-R$ plane: (a) effect of the v parameter for $\chi N = 30$; (b) effect of χN for $v = 0.1$.

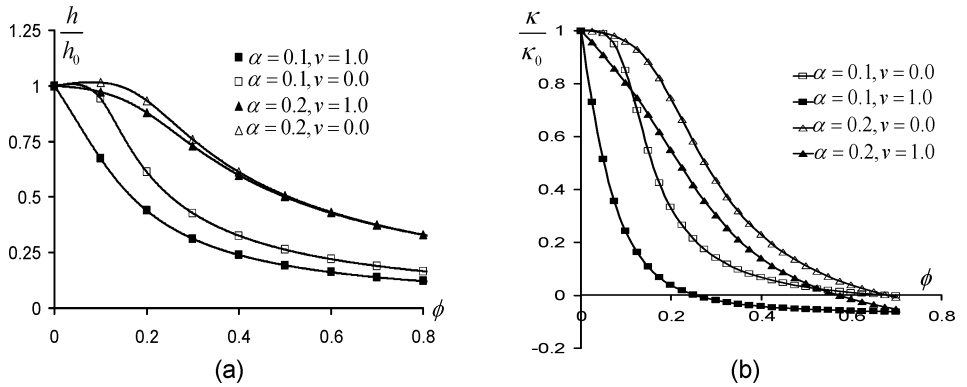

Figure 9. (a) Effect of a nonzero v parameter (fluctuation corrections) upon the height of the brush h (normalized by its value in the absence of the particles). (b) Effect of a nonzero v parameter (fluctuation corrections) upon the bending modulus of the layer κ (normalized by its value in the absence of the particles).

also drawn in a comparison of the relative locations of the thickness and bending modulus related instabilities (not displayed).

V. Computer Simulation of Copolymer−Nanoparticles System

A. Simulation Details. Much of our above theoretical analysis was inspired by preliminary computer simulation results of a block copolymer−nanoparticle system. To test our model predictions, we carried out constant pressure ensemble computer simulations[48] of a block copolymer−nanoparticle system. However, considering the limited range of validity of strong segregation theory, only a qualitative comparison with our simulations could be achieved. In this section, we present in brief our results for the case of surfactant-like particles considered in the previous section. Qualitative tests of our predictions in section III have already been furnished in experiments and alternate theories discussed earlier.

The equilibrium and dynamics of our model system are simulated by a recently proposed variant of the momentum-conserving Dissipative particle dynamics (DPD) approach.[49] Our earlier articles have presented a detailed description of the simulation methodology and the functional form of the interaction potentials for polymer−particle system. To maintain brevity, we refrain from repeating them here. For our simulations, the size of the polymer segment was chosen as the fundamental length scale for normalizing the lengths in the simulation. For the present situation, we simulated two symmetric diblock copolymers of the kind A_6B_6 and $A_{12}B_{12}$. The (unperturbed) radius of gyration of these polymers was found to satisfy Gaussian statistics with a statistical segment length of 1.5. The total number of polymer segments in the simulation cell was fixed at 7680, and the particle concentration was varied by the addition of particles of a fixed radius of 2.25 units. We studied polymer−nanoparticle composite systems with 1, 8, 16, and 32 particles corresponding to volume fractions Φ of 0.01, 0.06, 0.11, and 0.21, respectively.

The interactions between the A and B segments were parametrized to provide high incompatibility and segregation between blocks. In the parametric notation of our earlier article,[50] we chose the interaction parameter $a_{AB} = 550$ for $N = 24$ and $a_{AB} = 1850$ for $N = 12$. We then used the equilibrium thickness of the lamella to parametrize the χ_{AB} (values discussed below) corresponding to the parameters of our potential. To mimic the "nonselective" particle situation considered in the previous section, we considered particles which were equally selective to both A and B phases of the polymer. Selectivity was incorporated into the potentials by the addition of an attractive interaction between the polymer segment and the particle. Explicitly, the polymer segment−particle potential (eq A4 in our earlier article) is now modified as

$$\mathbf{F}_{SC}^{(C)}(\mathbf{r}) = \begin{cases} \dfrac{12\epsilon_{SC}\sigma_{SC}^{6}}{r^{8}}\alpha_{SC} - \dfrac{\sigma_{SC}^{6}}{r^{6}}\mathbf{r} & r < r_{SC} \\ 0 & r < r_{SC} \end{cases} \tag{35}$$

where we set $\alpha_{SC} = 1$ to mimic the selective interactions. Using the above simulation parameters, the model parameters of the previous sections were estimated to be $R/R_g = 0.75$, $R_g = 3$, $h_0 = 4.4$, $\alpha = 0.35$, $\chi N_p \simeq 25 \pm 5$, and $v = 0.9$ for $N = 24$ and $R/R_g = 1.06$, $R_g = 2.12$, $v = 1.2$, $h_0 = 4.3$, $\alpha = 0.49$, and $\chi N \simeq 28 \pm 5$ for $N = 12$.

The simulations were started from random initial conditions of the particle and polymer segment positions and were

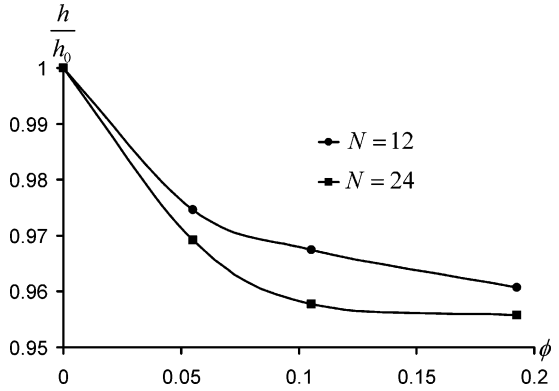

Figure 10. Lamella thickness h (relative to its value in the absence of particles h_0) as a function of particle concentration ϕ.

equilibrated by applying a weak periodical field (with a period commensurate with the cell size) to align the lamella along one of the faces of the periodical cell (henceforth referred to as the z direction). Subsequently, we turned off the field, and we allowed the system to relax for a short time and calculated the anisotropy of the stresses:

$$\delta\sigma = 2\sigma_{zz} - \sigma_{xx} - \sigma_{yy} \tag{36}$$

where σ_{ij} denotes the ijth component of the stresses. If $\delta\sigma$ was positive (negative), we stretched (compressed) the cell in the z direction and compressed (stretched) it in the xy plane so as to keep the volume to be constant. Subsequently, the system was relaxed and the anisotropy in stresses were checked and the procedure was repeated. This procedure eventually leads to a lamella aligned along the z direction with an isotropic stress tensor σ which we consider the aligned "quasi-equilibrium" lamella structure. The thickness of the above-aligned lamella is taken to be the "equilibrium" lamella thickness corresponding to the nanoparticle loading Φ. The system is then evolved further to allow it to manifest any instabilities which may result for the given conditions.

B. Simulation Results. Displayed in Figure 10 are the equilibrium heights of an initially aligned lamella as a function of the particle loading Φ. Consistent with the predictions displayed in Figures 4 and 9, we observe that the lamella period decreases monotonically with an increase in particle loading. We note that the values of α in our simulation are relatively large ($\alpha = 0.49$ for $N_p = 12$ and $\alpha = 0.35$ for $N_p = 24$), and hence the contraction of lamella thickness is considerably lower than those portrayed in Figure 9. However, the qualitative trend of our simulation results (stronger contraction for lower values of α) is in agreement with our model predictions.

Time evolution of the initially aligned lamella structure lends support to the second of our predictions, viz., that the addition of a sufficient loading of nonselective particles transforms the aligned lamella into a disordered albeit segregated lamella. Figure 11 displays simulation snapshots of the particle and polymer conformations for $\Phi = 0.06$ and $N = 12$. The upper panel displays the initially aligned configuration, with the left and right panels displaying just the A and B blocks along with the particles. One can see that initially the particles tend to be localized at the AB interfaces. The lower panel displays the final configuration after evolution of the system over a long simulation run. One can see that the system evolves to a disordered, albeit segregated phase. The segregated nature is evident in the snapshot displayed in the middle panel, whereas the disordered nature of the phases is evident in the snapshots of the configurations of the A and B segments displayed in the left and right panels. A more quantitative verification of the disordering is presented in the 1D averaged density profiles displayed in Figure 12. It is evident that for $\Phi = 0.01$ the density profiles suggest preferential localization near AB interfaces, while the plots for $\Phi = 0.06$ demonstrate the disordering of the lamella structure. A similar effect is also seen in the density profiles for $N_P = 24$ displayed in Figure 12c,d, where again it is seen that at the highest concentration of $\Phi = 0.21$ that the lamella becomes disordered.

To contrast the above results with that of the selective particles, we also performed simulations with the particle just nonselective with the A phase of the polymer ($\alpha_{CS} = 1$ for A segments and $\alpha_{CS} = 0$ for B segments). Shown in Figure 13 are the simulation snapshots for $N_C = 32$ and the corresponding

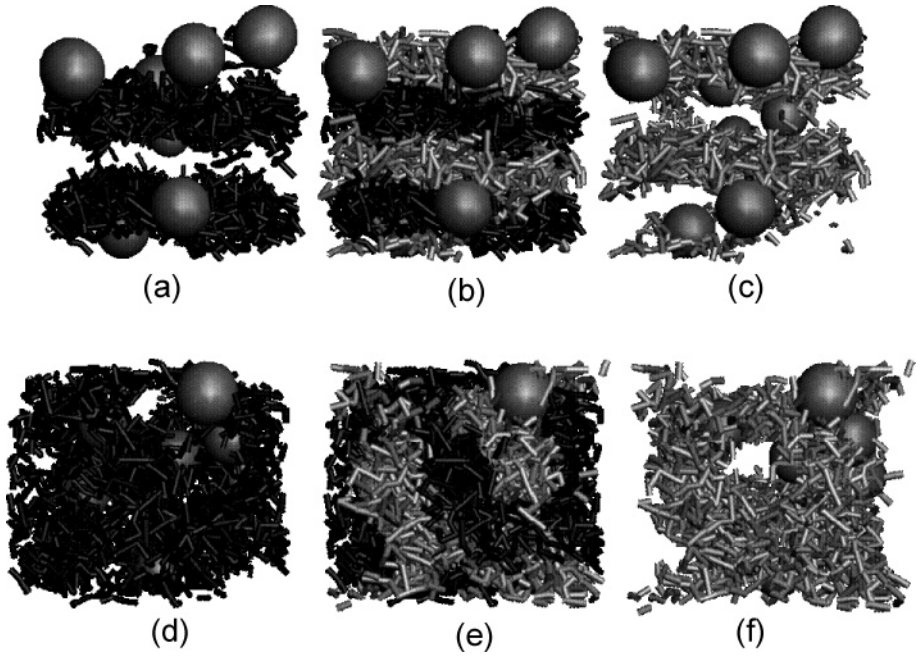

Figure 11. Snapshots of diblock copolymer composites for $N = 12, \Phi = 0.06$. (a)−(c) represent the initial configurations of (a) A component + particles, (b) A + B components + particles, and (c) B component + particles. (d)−(f) represent the final configurations configuration after 10^5 time steps of (d) A component + particles, (e) A + B components + particles, and (f) B component + particles.

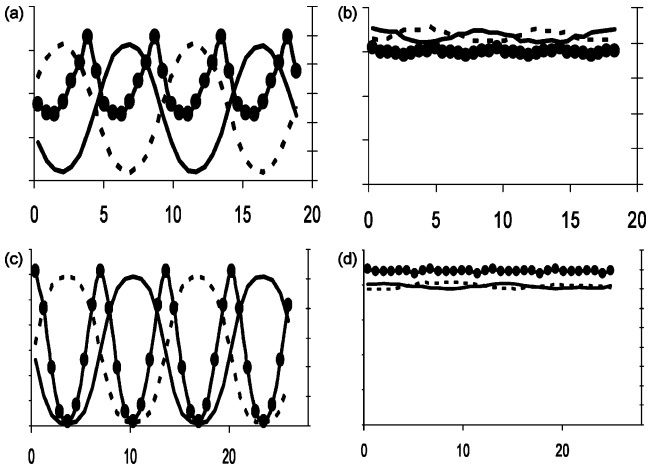

Figure 12. Averaged density profiles for mixtures of diblocks and nonselective particles (solid lines, A component; dotted lines, B component; solid lines with circles, particles): (a) $N = 12$, $\Phi = 0.01$; (b) $N = 12$, $\Phi = 0.06$; (c) $N = 24$, $\Phi = 0.01$; (d) $N = 24$, $\Phi = 0.21$.

averaged density profiles. It is clear that in this case the lamellar ordering as well the particle segregation remains intact up to the highest particle concentration probed.

VI. Summary and Outlook

We presented a strong segregation approximation based theory for ordering in mixtures of symmetric block copolymer and nanoparticles. The first section considered the case of dilute concentrations of nanoparticles and presented predictions for the density profiles of both selective and nonselective nanoparticles. Also, the role of particles in influencing the lamella thickness was also considered. It was shown that nonselective particles tend to localize near the interface and contract the lamella thickness. In contrast, it was shown that the selective particles tend to segregate into its preferred phase, with the segregation increasing with increasing size. These results were shown to match with experiments and earlier theories, but our predictions provided a quantification of the parameters determining the segregation. In conjunction with an experimental quantification of the density profiles and/or the lamella thicknesses, our model provides the means to parametrize the particle−polymer interactions and predict the characteristics for other conditions.

We then considered the case of finite concentration of particles and presented a more accurate treatment of the particle size effects to identify their effects upon the characteristics of the block copolymer layer. We specifically focused on the case of nonselective particles where we used an Alexander−DeGennes approximation to discern the lamella height and the elastic constants as a function of the concentration of the particles. We demonstrated that, in general, the addition of particles leads to a contraction of the lamella and a lowering of the bending modulii. We pointed out that the possibility of different layer instabilities which can result from these effects. Finally, we presented simulation results confirming the qualitative features of our predictions.

Our results in the second section suggest that while block copolymers have been traditionally viewed as the "supramolecular surfactant", nonselective nanoparticles can act as surfactant for the block copolymer phases themselves and aid in the formation of segregated, nanosized bicontinuous structures—a phase morphology which has the potential for many applications and has attracted significant interest.[20,51,52] We note that after the present article was submitted for publication we received a preprint from Kramer and co-workers,[21] which semiquantitatively validates many of our scaling predictions and the formation of bicontinuous morphologies in nonselective nanoparticle−block copolymer mixtures.

Many future directions arise from our work. The case of asymmetric polymers and/or self-assembly transitions between

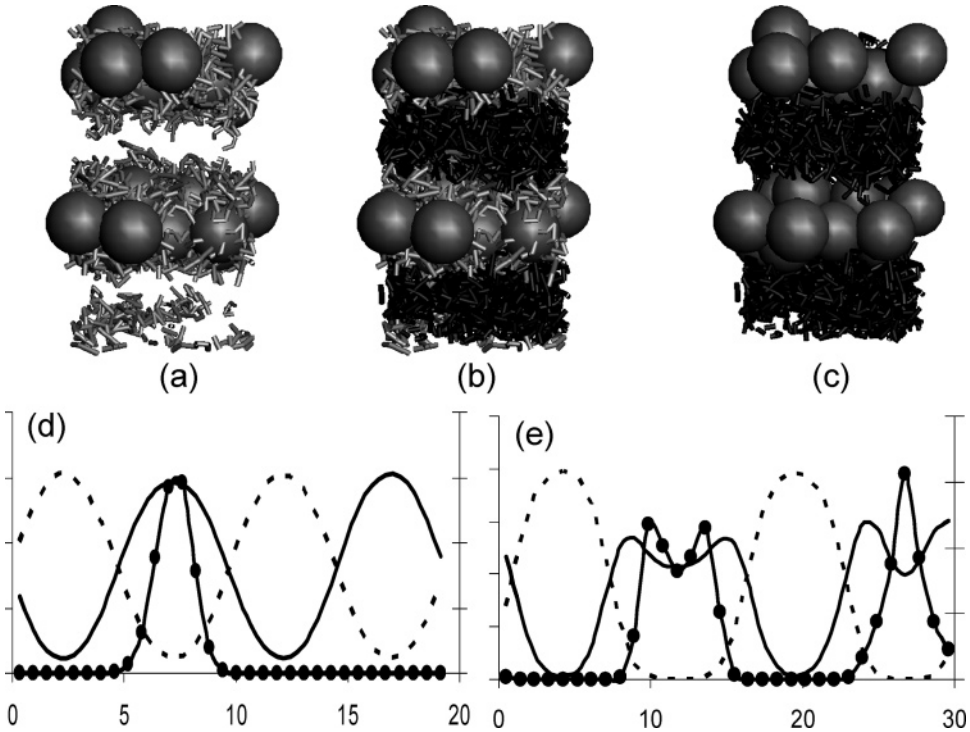

Figure 13. Snapshots of diblock copolymer composites for $N = 24$, $\Phi = 0.21$ and selective particles. (a)−(c) represent the final configurations of (a) A component + particles, (b) A + B components + particles, and (c) B component + particles. Averaged density profiles for mixtures of diblocks and selective particles (solid lines, A component; dotted lines, B component; solid lines with circles, particles): (d) $N = 24$, $\Phi = 0.01$; (e) $N = 24$, $\Phi = 0.21$.

lamella and cylinders, etc., can also be treated within the strong segregation approximation.[24,30] The case of selective particles is of equal, if not more, interest from the experimental side.[25] A treatment of this case along the lines of this work proves a little more complex due to the need to account for the changes in the free end distribution which results from the positioning of the particle. In the limit of small particles, such effects might not prove so relevant, allowing one to map the system to that of a diblock copolymer in a selective solvent. The latter has been studied extensively from both experimental and theoretical point of view.[53−55] Unfortunately, the case of larger particles is more complicated and might need numerical calculations to discern the resulting thermodynamic characteristics.

Acknowledgment. This work was supported in part by a Sloan Fellowship by the Alfred P. Sloan Foundation, by a grant from Robert A. Welch Foundation, and by the National Science Foundation under Award NSF CTS-0347381. We gratefully acknowledge the allocation of computer time in Texas Advanced Computing Center. We also thank Profs. Zheng-Gang Wang, Glenn Fredrickson, Ed Kramer, and Anna Balazs for stimulating comments and discussions regarding different aspects of this manuscript.

References and Notes

(1) Bockstaller, M. R.; Lapetnikov, Y.; Margel, S.; Thomas, E. L. *J. Am. Chem. Soc.* **2003**, *125*, 5276.
(2) Haryono, A.; Binder, W. H. *Small* **2006**, *2*, 600.
(3) Bockstaller, M. R.; Mickiewicz, R. A.; Thomas, E. L. *Adv. Mater.* **2005**, *17*, 1331.
(4) Chiu, J. J.; Kim, B. J.; Kramer, E. J.; Pine, D. J. *J. Am. Chem. Soc.* **2005**, *127*, 5036.
(5) Hashimoto, T.; Harada, M.; Sakamoto, N. *Macromolecules* **1999**, *32*, 6867.
(6) Leppert, V. J.; Murali, A. K.; Risbud, S. H.; Stender, M.; Power, P. P.; Nelson, C.; Banerjee, P.; Mayes, A. M. *Philos. Mag. B* **2002**, *82*, 1047.
(7) Lauter-Pasyuk, V.; Lauter, H. J.; Gordeev, G. P.; Muller-Buschbaum, P.; Toperverg, B. P.; Jernenkov, M.; Petry, W. *Langmuir* **2003**, *19*, 7783.
(8) Kim, B. J.; Chiu, J. J.; Yi, G. R.; Pine, D. J.; Kramer, E. J. *Adv. Mater.* **2005**, *17*, 2618.
(9) Kim, B.; Bang, J.; Hawker, C.; Kramer, E. *Macromolecules* **2006**, *39*, 4108.
(10) Jain, A.; Gutmann, J. S.; Garcia, C. B. W.; Zhang, Y. M.; Tate, M. W.; Gruner, S. M.; Wiesner, U. *Macromolecules* **2002**, *35*, 4862.
(11) Hanley, K. J.; Lodge, T. P.; Huang, C. I. *Macromolecules* **2000**, *33*, 5918.
(12) Bockstaller, M. R.; Thomas, E. L. *Phys. Rev. Lett.* **2004**, *93*, article 166106.
(13) Ginzburg, V. V.; Gibbons, C.; Qiu, F.; Peng, G. W.; Balazs, A. C. *Macromolecules* **2000**, *33*, 6140.
(14) Huh, J.; Ginzburg, V. V.; Balazs, A. C. *Macromolecules* **2000**, *33*, 8085.
(15) Thompson, R. B.; Ginzburg, V. V.; Matsen, M. W.; Balazs, A. C. *Science* **2001**, *292*, 2469.
(16) Thompson, R. B.; Ginzburg, V. V.; Matsen, M. W.; Balazs, A. C. *Macromolecules* **2002**, *35*, 1060.
(17) Schultz, A. J.; Hall, C. K.; Genzer, J. *Macromolecules* **2005**, *38*, 3007.
(18) Sides, S. W.; Kim, B. J.; Kramer, E. J.; Fredrickson, G. H. *Phys. Rev. Lett.* **2006**, *96*, article 250601.
(19) Lopes, W. A. *Phys. Rev. E* **2002**, *65*, article 031606.
(20) Krishnan, K.; Almdal, K.; Burghardt, W. R.; Lodge, T. P.; Bates, F. S. *Phys. Rev. Lett.* **2001**, *87*, article 098301.
(21) Kim, B. J.; Fredrickson, G. H.; Hawker, C. J.; Kramer, E. J. Nanoparticle Surfactants as a Route to Bicontinuous Block Copolymer Morphologies. Preprint, 2006.
(22) Roux, D.; Coulon, C.; Cates, M. E. *J. Phys. Chem.* **1992**, *96*, 4174.
(23) Porte, G.; Appell, J.; Bassereau, P.; Marignan, J. *J. Phys. (Paris)* **1989**, *50*, 1335.
(24) Lee, J. Y.; Shou, Z.; Balazs, A. C. *Phys. Rev. Lett.* **2003**, *91*, 136103.
(25) Lee, J. Y.; Shou, Z. Y.; Balazs, A. C. *Macromolecules* **2003**, *36*, 7730.
(26) Kim, J. U.; O'Shaughnessy, B. *Phys. Rev. Lett.* **2002**, *89*.
(27) Kim, J. U.; O'Shaughnessy, B. *Macromolecules* **2006**, *39*, 413.
(28) Williams, D. R. M.; Pincus, P. A. *Europhys. Lett.* **1993**, *24*, 29.
(29) Ganesan, V.; Fredrickson, G. H. *Europhys. Lett.* **2001**, *55*, 814.
(30) Semenov, A. N. *Zh. Eksp. Teor. Fiz.* **1985**, *88*, 1242.
(31) Helfand, E.; Tagami, Y. *J. Polym. Sci., Polym. Lett.* **1971**, *9*, 741.
(32) Leibler, L. *Macromolecules* **1980**, *13*, 1602.
(33) Matsen, M. W.; Schick, M. *Phys. Rev. Lett.* **1994**, *72*, 2660.
(34) Halperin, A.; Tirrell, M.; Lodge, T. P. *Adv. Polym. Sci.* **1992**, *100*, 31.
(35) Szleifer, I.; Carignano, M. A. *Adv. Chem. Phys.* **1996**, *94*, 165.
(36) Netz, R. R.; Schick, M. *Macromolecules* **1998**, *31*, 5105.
(37) Alexander, S. *J. Phys. (Paris)* **1977**, *38*, 983.
(38) Degennes, P. G. *Macromolecules* **1980**, *13*, 1069.
(39) Milner, S. T.; Witten, T. A.; Cates, M. E. *Macromolecules* **1988**, *21*, 2610.
(40) Zhulina, Y. B.; Pryamitsyn, V. A.; Borisov, O. V. *Vysokomol. Soedin., Ser. A* **1989**, *31*, 185.
(41) Milner, S. T.; Witten, T. A. *J. Phys. (Paris)* **1988**, *49*, 1951. Wang, Z. G.; Safran, S. A. *J. Chem. Phys.* **1991**, *94*, 679.
(42) Matsen, M. W. *J. Chem. Phys.* **1999**, *110*, 4658.
(43) Williams, D. R. M. *J. Phys. II* **1993**, *3*, 1313.
(44) Zhulina, E. B.; Birshtein, T. M.; Priamitsyn, V. A.; Klushin, L. I. *Macromolecules* **1995**, *28*, 8612.
(45) Pryamitsyn, V.; Ganesan, V. *J. Chem. Phys.* **2004**, *120*, 5824.
(46) Morse, D. C. *Phys. Rev. E* **1994**, *50*, R2423.
(47) Morse, D. C. *Curr. Opin. Colloid Interface Sci.* **1997**, *2*, 365.
(48) Allen, M. P.; Tildesley, D. J. *Computer Simulation of Liquids*; Oxford University Press: New York, 1987.
(49) Pryamitsyn, V.; Ganesan, V. *J. Chem. Phys.* **2005**, *122*, 104906.
(50) Pryamitsyn, V.; Ganesan, V. *Macromolecules* **2006**, *39*, 844.
(51) Finnefrock, A. C.; Ulrich, R.; Toombes, G. E. S.; Gruner, S. M.; Wiesner, U. *J. Am. Chem. Soc.* **2003**, *125*, 13084.
(52) Chung, H.; Ohno, K.; Fukuda, T.; Composto, R. J. *Nano Lett.* **2005**, *5*, 1878.
(53) Laicer, C. S. T.; Chastek, T. Q.; Lodge, T. P.; Taton, T. A. *Macromolecules* **2005**, *38*, 9749.
(54) Naughton, J. R.; Matsen, M. W. *Macromolecules* **2002**, *35*, 5688.
(55) Birshtein, T. M.; Zhulina, E. B. *Polymer* **1990**, *31*, 1312.

MA0613382